Universität des Saarlandes

Fachrichtung 6.1 – Mathematik

Tensor Field Interpolation with PDEs

Joachim Weickert and Martin Welk

Tensor Field Interpolation with PDEs

Joachim Weickert

Mathematical Image Analysis Group
Faculty of Mathematics and Computer Science
Saarland University, Building 27
66041 Saarbrücken, Germany
weickert@mia.uni-saarland.de

Martin Welk

Mathematical Image Analysis Group
Faculty of Mathematics and Computer Science
Saarland University, Building 27
66041 Saarbrücken, Germany
welk@mia.uni-saarland.de

Edited by
FR 6.1 – Mathematik
Universität des Saarlandes
Postfach 15 11 50
66041 Saarbrücken
Germany

Fax: + 49 681 302 4443
e-Mail: preprint@math.uni-sb.de
WWW: http://www.math.uni-sb.de/

Abstract

We present a unified framework for interpolation and regularisation of scalar- and tensor-valued images. This framework is based on elliptic partial differential equations (PDEs) and allows rotationally invariant models. Since it does not require a regular grid, it can also be used for tensor-valued scattered data interpolation and for tensor field inpainting. By choosing suitable differential operators, interpolation methods using radial basis functions are covered. Our experiments show that a novel interpolation technique based on anisotropic diffusion with a diffusion tensor should be favoured: It outperforms interpolants with radial basis functions, it allows discontinuity-preserving interpolation with no additional oscillations, and it respects positive semidefiniteness of the input tensor data.

Keywords: matrix-valued images, interpolation, inpainting, scattered data interpolation, regularisation, partial differential equations, nonlinear diffusion.

Contents

1 Introduction

Many tasks in image processing, computer vision and computer graphics require to interpolate or resample images in order to obtain data at locations that do not coincide with the grid points where the digital image values are known. Classical methods to achieve this goal are linear interpolation, cubic or quintic splines, radial basis functions and sinc-based interpolation techniques; see e.g. [10, 13]. If the data are not available on a regular grid, scattered data interpolation techniques have been proposed [7, 15]. More recently, also interpolation methods based on variational formulations and nonlinear partial differential equations (PDEs) have been advocated [4, 11], in particular for so-called inpainting methods [12, 5, 9], where the image data are only corrupted in specific areas. Nonlinear PDEs allow to design discontinuity-preserving interpolants.

While image interpolation is fairly well-understood for scalar images, not much research has been done so far with respect to interpolation of matrix fields. Aldroubi and Basser [1] have proposed sampling in shift invariant amalgam spaces, while Pajevic et al. [16] study B-splines and non-uniform rational B-splines for interpolating tensor fields. Moakher and Batchelor [14] investigate the Riemannian symmetric space of positive definite tensors and propose interpolation strategies that respect positive definiteness. Suarez-Santana et al. [18] use a convolution-based interpolation with structure-adaptive weights. No attempts, however, have been made so far to study nonlinear PDE-based interpolation schemes for tensor fields. This is the goal of the present paper.

The paper is organised as follows. In Section 2 we first consider the scalar case. We review splines as minimisers of suitable energy functionals whose Euler–Lagrange equations lead to elliptic PDEs. By showing that variational image restoration methods lead to similar PDEs, we derive a novel unified model for image approximation and interpolation. This unified model is extended to the tensor framework in Section 3. It covers linear and nonlinear PDEs of arbitrary order. Experiments are presented with data sets from DT-MRI and computational fluid dynamics that demonstrate the properties of the different PDE interpolants. The paper is concluded with a summary in Section 4.

2   Scalar Interpolation

2.1   Spline Interpolation

Let us start our considerations with one of the most important scalar interpolation methods: spline interpolation in 1-D. Assume we are given some interpolation points $0 = x_1 < x_2 < ... < x_n = 1$ with function values $f(x_1),...,f(x_n)$. For performing spline interpolation we are seeking a smooth function $u(x) : [0, 1] \to \mathbb{R}$ that minimises

$$E(u) = \int_0^1 (\partial_x^m u)^2 \, dx \tag{1}$$

subject to

$$u(x_i) = f(x_i) \qquad (i = 1,...,n). \tag{2}$$

It is well-known that this gives linear interpolation for $m = 1$. In this case we have continuity, i.e. C^0-smoothness at the interpolation points. For $m = 2$ we obtain cubic spline interpolation, with C^2-smoothness at the interpolation points, and $m = 3$ gives quintic spline interpolation with C^4-smoothness. In general, we get spline interpolation of degree $2m-1$ with C^{2m-2}-smoothness.

A necessary condition for minimising (1) is given by the Euler–Lagrange equation $(-1)^{m+1} \partial_{xx}^m u = 0$. Together with the interpolation constraints (2), we can cast both conditions in a single equation:

$$c(x) \cdot \underbrace{(u(x) - f(x))}_{\text{interpolation}} - (1 - c(x)) \cdot \underbrace{(-1)^{m+1} \partial_{xx}^m u}_{\text{smoothness}} = 0 \tag{3}$$

with

$$c(x) := \begin{cases} 1 & \text{if } x \in \{x_0, ..., x_n\} \\ 0 & \text{else.} \end{cases} \tag{4}$$

This is a linear PDE of order $2m$. For large m, we obtain a very smooth solution, but in general we can expect no maximum–minimum principle for $m > 1$. As a consequence, the interpolating spline may give over- and undershoots, i.e. there is no guarantee that it remains within the convex hull of the data. This can be very undesirable in a number of applications. The case $m = 1$, on the other hand, is not very exciting since it leads to simple linear interpolations which are not sufficiently smooth for many purposes. However, later on we shall see that it can be attractive to stick to the case $m = 1$, if we permit *nonlinear anisotropic* PDEs instead of *linear* ones.

2.2 Regularisation

It is instructive to complement our considerations on *interpolation* by an important *approximation* paradigm, namely variational regularisation methods. In 1-D, they can be introduced as follows. Given some noisy signal $f : [0,1] \to \mathbb{R}$, we want to find a signal u that minimises an energy functional that rewards similarity between $u(x)$ and $f(x)$, as well as smoothness of $u(x)$:

$$E(u) = \int_0^1 \Big(c \cdot \underbrace{(u-f)^2}_{\text{similarity}} + (1-c) \cdot \underbrace{\Psi(u_x^2)}_{\text{smoothness}} \Big) dx \qquad (5)$$

with some weight $0 < c < 1$ and an increasing penalising function $\Psi : [0,\infty) \to \mathbb{R}$. This leads to the Euler–Lagrange equation

$$c \cdot (u - f) - (1-c) \cdot \partial_x \big(\Psi'(u_x^2)\, u_x \big) = 0 \qquad (6)$$

with homogeneous Neumann boundary conditions. In general, this is a nonlinear PDE of order 2 that satisfies a maximum–minimum principle. The nonlinear penaliser $\Psi(u_x^2)$ allows discontinuity preserving smoothing. The total variation (TV) penaliser [17] e.g. is given by $\Psi(u_x^2) = 2|u_x|$. It leads to an Euler–Lagrange equation with the TV diffusivity $g(u_x^2) := \Psi'(u_x^2) = \frac{1}{|u_x|}$. It reduces smoothing at locations where the gradient magnitude is large.

2.3 A Unified Model

The PDE interpretation of spline interpolation and regularisation allows us now to study a unified model for image interpolation and approximation. Let $\Omega \subset \mathbb{R}^n$ denote our n-dimensional image domain and assume we are given some incomplete or noisy scalar image data $f : \Omega \to \mathbb{R}$. Then we propose to obtain an interpolated or processed image u that satisfies

$$c(x) \cdot (u - f) - (1 - c(x)) \cdot Lu = 0 \qquad (7)$$

with a *confidence function* $c(x) : \Omega \to [0,1]$, some elliptic differential operator L, and homogeneous Neumann boundary conditions.

Let us first analyse the confidence function $c(x)$. This function allows to fill in missing data at locations x where $c(x) = 0$, while $u(x)$ reproduces $f(x)$ at locations where $c(x) = 1$. Consequently, we can use this model for interpolation by simply setting c to 0 or 1. It should be noted that the locations x where $c(x) := 1$ do not necessarily have to be on a regular grid: The model is equally valid for scattered data interpolation and inpainting.

4

At locations where we choose $0 < c(x) < 1$, we obtain an approximation by regularisation. For classical regularisation, c is fixed. However, $c(x)$ expresses the confidence in the data. It can be chosen e.g. such that it is inversely proportional to the local noise variance of f, if there are indications that the data are not equally reliable at different locations. Hence we have a very flexible method for denoising (approximation) with simultaneous filling-in of data (interpolation).

Regarding the elliptic differential operator L, many possibilities exist. Inspired from spline interpolation, a suitable n-dimensional generalisation of (3) would use the Laplacian operator (also called harmonic or linear diffusion operator) $Lu := \Delta u$ for $m = 1$, the biharmonic operator $Lu := -\Delta^2 u$ for $m = 2$, or the triharmonic operator $Lu := \Delta^3 u$ for $m = 3$. These linear operators correspond to interpolation with radial basis functions [3]. From the theory of nonlinear diffusion filtering, on the other side, it would be interesting to use the isotropic nonlinear operator $Lu := \mathrm{div}\left(g(|\nabla u|^2)\nabla u\right)$ or its anisotropic counterpart[1] $Lu := \mathrm{div}\left(g(\nabla u_\sigma \nabla u_\sigma^\top)\nabla u\right)$, where u_σ is a Gaussian-smoothed version of u, and g is a decreasing positive diffusivity function. The isotropic operator reduces diffusion at edges of u_σ, while the anisotropic one permits diffusion along edges of u_σ and reduces diffusion across edges of u_σ. For more details on nonlinear diffusion the reader is referred to [20]. Note that only the second-order differential operators allow a maximum–minimum principle, where the values of u stay within the range of the values that f takes at locations where $c(x) > 0$. One should also note that all these differential operators are rotationally invariant, unlike a number of popular interpolation techniques such as multivariate spline interpolation.

2.4 Experiments

Let us now evaluate the quality of our unified model (7) in the case of scalar image interpolation. To this end we extract the solutions of the elliptic PDEs as steady states of corresponding parabolic evolutions that are discretised by an explicit (Euler forward) finite difference scheme.

Figure 1 shows a test image and a sparsified version where only 1 out of 64 pixels is used. Based on this sparsified image, interpolation with various differential operators and optimised parameters is shown in Fig. 2. In the

---

[1]A scalar-valued function $g(x)$ is extended to a matrix-valued function $g(A)$ by applying g to the eigenvalues on A and leaving the eigenvectors unchanged.

Figure 1: (a) **Left:** Original image. (b) **Right:** Data points for interpolation. Only 1 out of 64 points is used.

nonlinear diffusion cases, a Charbonnier diffusivity [6] is used:

$$g(s^2) = \frac{1}{1 + s^2/\lambda^2} \tag{8}$$

with some contrast parameter $\lambda > 0$. Quantitative results in terms of the average Euclidean distance

$$\mathrm{AED}\,(u, v) \ := \ \Big(\frac{1}{|\Omega|} \int_\Omega (u(x) - v(x))^2 \, dx\Big)^{1/2} \tag{9}$$

between the interpolated image u and its ground truth v are given in Table 1. We observe that linear diffusion performs worst and is significantly worse than isotropic nonlinear diffusion. Biharmonic and triharmonic smoothing give fairly good results, but blur image edges and show oscillations near them. They also violate a maximum–minimum principle. Anisotropic diffusion performs best: It gives the highest SNR. It also obeys a maximum–minimum principle, respects discontinuities and does not suffer from visible oscillations.

3 Tensor Interpolation

3.1 PDE Formulations

Let us now investigate how the scalar PDE-based interpolation techniques from the previous section can be extended to the tensor case.

6

Figure 2: Scalar-valued interpolation of Fig. 1(b). (a) **Top Left:** Interpolation data. (b) **Top Middle:** Interpolation with linear diffusion. (c) **Top Right:** Isotropic nonlinear diffusion. (d) **Bottom Left:** Anisotropic nonlinear diffusion. (e) **Bottom Middle:** Biharmonic smoothing. (f) **Bottom Right:** Triharmonic smoothing.

For the linear PDEs, extensions to the tensor framework are straightforward: Harmonic (linear diffusion), biharmonic and triharmonic smoothing can be

Table 1: Interpolation quality of the scalar-valued methods from Fig. 2. AED = average Euclidean distance to the correct image.

smoothing operator	AED	max.–min. principle
linear diffusion	19.80	yes
isotropic nonlinear diffusion	18.42	yes
anisotropic nonlinear diffusion	15.16	yes
biharmonic smoothing	15.76	no
triharmonic smoothing	16.36	no

applied componentwise leading to

$$c(x)(u_{ij} - f_{ij}) - (1 - c(x))\,\Delta^1 u_{ij} = 0 \quad \text{(harmonic)} \tag{10}$$

$$c(x)(u_{ij} - f_{ij}) + (1 - c(x))\,\Delta^2 u_{ij} = 0 \quad \text{(biharmonic)} \tag{11}$$

$$c(x)(u_{ij} - f_{ij}) - (1 - c(x))\,\Delta^3 u_{ij} = 0 \quad \text{(triharmonic)} \tag{12}$$

for a tensor image $F = (f_{ij}) : \Omega \to \mathbb{R}^{n \times n}$ and its interpolant $U = (u_{ij})$. The fact that biharmonic and triharmonic smoothing violate a maximum–minimum principle in the scalar setting has an interesting consequence in the tensor framework: The interpolated tensor field may not be positive semidefinite (PSD), even if all tensors at locations x with $c(x) > 0$ are positive semidefinite. This may be a drawback for applications such as diffusion tensor MRI.

In the nonlinear diffusion setting where discontinuities are to be preserved, a suitable channel coupling is natural. We can design interpolation methods by applying recent tensor-valued extensions of nonlinear diffusion filtering in the isotropic [19] and anisotropic case [21]: In the isotropic case, channel coupling is achieved by a joint diffusivity leading to

$$c(x)\,(u_{ij} - f_{ij}) - (1 - c(x))\,\text{div}\left(g\left(\sum_{k,l} |\nabla u_{kl}|^2\right) \nabla u_{ij}\right) = 0. \tag{13}$$

In the anisotropic case, a joint diffusion tensor is used:

$$c(x)\,(u_{ij} - f_{ij}) - (1 - c(x))\,\text{div}\left(g\left(\sum_{k,l} \nabla u_{kl,\sigma} \nabla u_{kl,\sigma}^{\top}\right) \nabla u_{ij}\right) = 0. \tag{14}$$

Interestingly, one can show that such a channel coupling allows PSD preservation for these second-order PDEs, both in the continuous [2] and the discrete setting [21]. An intuitive explanation for this fact is given by the observation that coupled nonlinear diffusion can be regarded as a weighted averaging of matrices where identical (but space-variant) weights are used for all channels. If the matrices are positive semidefinite, then their weighted average is also positive semidefinite.

3.2   Experiments

For our experiments on tensor field interpolation we have created a synthetic 2-D test image that is depicted in Figure 3(a). The positive definite tensors are visualised by ellipses. Their colour is a function of the orientation of the ellipse and its anisotropy, such that an isotropic ellipse (a disk) appears white.

We perform two experiments where we evaluate the interpolation quality of the different tensor-valued PDEs: a zooming experiment where the interpolation points are equidistant, and a tensor-valued scattered data interpolation experiment. The corresponding interpolation data are given in Figs. 3(b) and (c), respectively.

For the zooming experiment the results for the different PDE-based interpolation methods are depicted in Figure 4. We observe that linear and isotropic nonlinear diffusion may create singularities at interpolation points near discontinuities. Biharmonic and in particular triharmonic interpolation, on the other hand, lead to visible oscillations. This can be seen best at the incorrect colours that are created in the white region. These artifacts reflect that fact that these equations are not PSD-preserving. Anisotropic nonlinear diffusion interpolation appears to be the best of both worlds: Since it is PSD-preserving, it does not introduce oscillatary artifacts. Moreover, it seems that is suffers less from singularities at interpolation points than linear and isotropic nonlinear diffusion interpolation.

The scattered data experiment in Figure 5 allows qualitively similar observations: Linear and isotropic nonlinear diffusion can exhibit singularities at interpolation points, while biharmonic and triharmonic interpolation create very disturbing oscillations. Once again, anisotropic nonlinear diffusion performs best.

In Table 2 we measure the difference between the interpolated tensor field $U = (u_{ij})$ and the ground truth $V = (v_{ij})$ for both experiments. This is done by computing the average Frobenius distance

$$\mathrm{AFD}\,(u,v) \; := \; \Big(\frac{1}{4\,|\Omega|} \sum_{i,j=1}^{2} \int_{\Omega} (u_{ij}(x) - v_{ij}(x))^2 \, dx \Big)^{1/2}, \qquad (15)$$

the tensorial analogue to the average Euclidean distance (9). The results confirm in both cases the visual impression that anisotropic nonlinear diffusion is the favourable interpolant for tensor fields.

4 Summary

We have presented a unified PDE model for regularisation and interpolation, both for scalar- and tensor-valued data. This framework allows rotationally invariant models and is not restricted to regular grids: It can also be used for scattered data interpolation and inpainting. Our experiments have shown

9
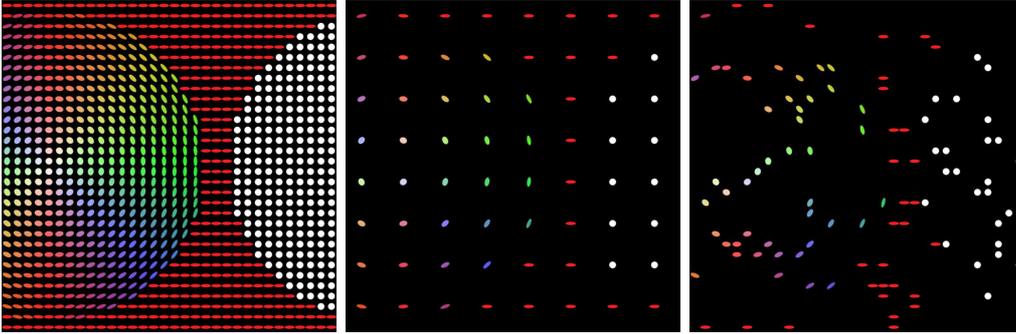
Figure 3: (a) **Left:** Synthetic 2-D tensor test image, 32×32 pixels. (b) **Middle:** Regular interpolation data where every fourth pixel in each direction is given. (c) **Right:** Scattered interpolation data where 10 percent of all pixels have been selected randomly.
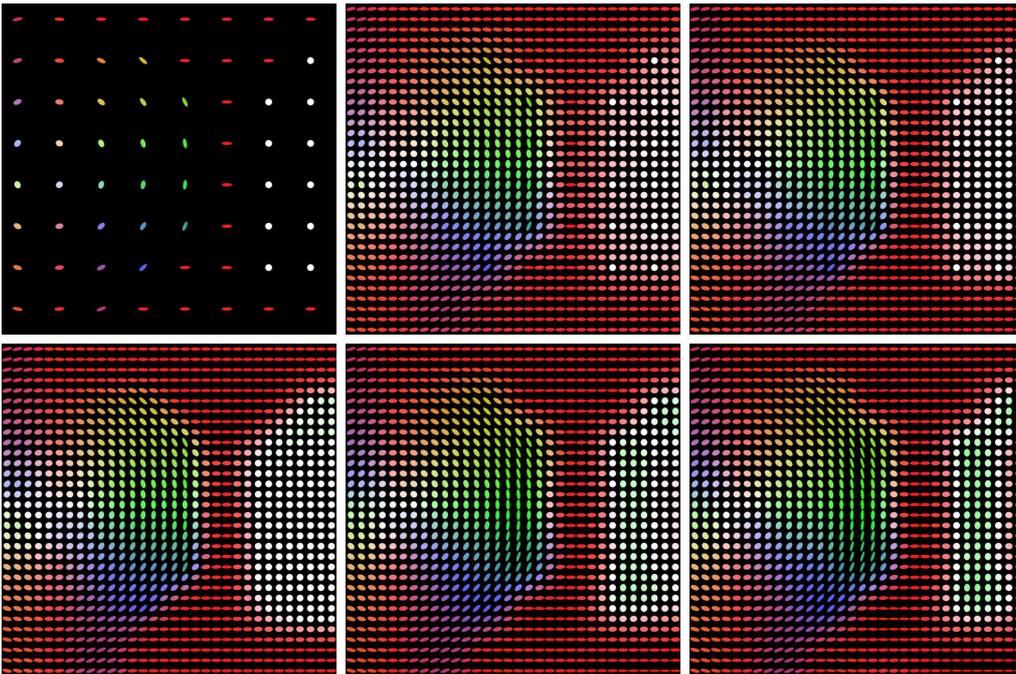
Figure 4: Tensor-valued interpolation of Fig. 3(b). (a) **Top left:** Interpolation data. (b) **Top middle:** Interpolation with linear diffusion. (c) **Top right:** Isotropic nonlinear diffusion. (d) **Bottom left:** Anisotropic nonlinear diffusion. (e) **Bottom middle:** Biharmonic smoothing. (f) **Bottom right:** Triharmonic smoothing.
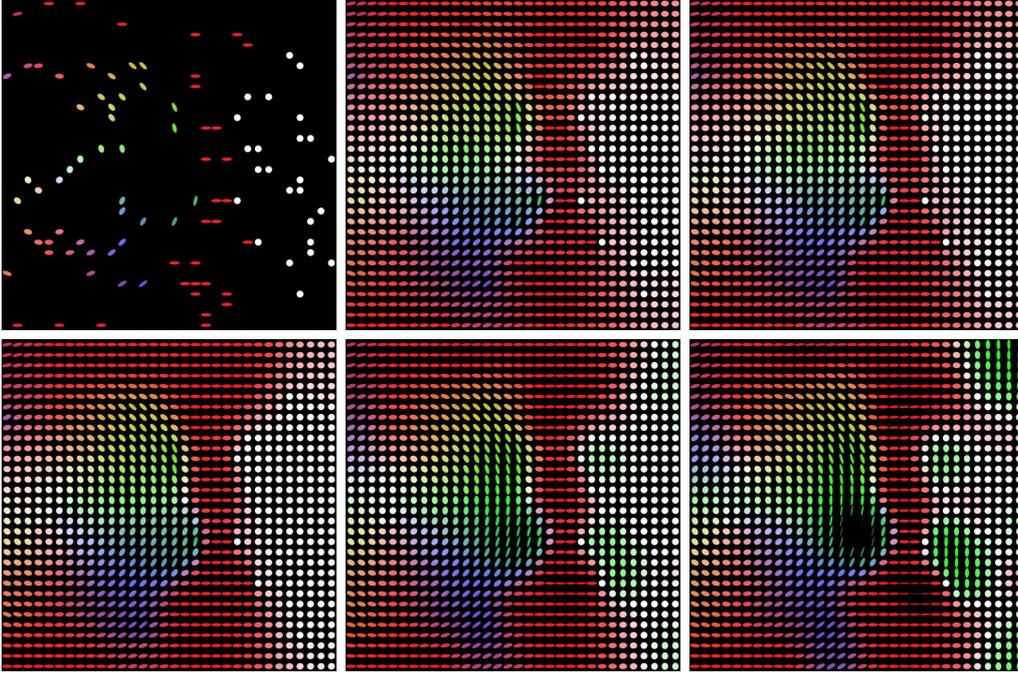
Figure 5: Tensor-valued scattered data interpolation of Fig. 3(c). (a) **Top left:** Interpolation data. (b) **Top middle:** Interpolation with linear diffusion. (c) **Top right:** Isotropic nonlinear diffusion. (d) **Bottom left:** Anisotropic nonlinear diffusion. (e) **Bottom middle:** Biharmonic smoothing. (f) **Bottom right:** Triharmonic smoothing.

Table 2: Interpolation quality of the tensor-valued interpolation experiments from Fig. 4 (zoom) and Fig. 5 (scattered data). Criteria are the average Frobenius difference (AFD) and preservation of positive semidefiniteness (PSD).

smoothing operator	AFD (zoom)	AFD (scattered)	PSD
linear diffusion	8.78	9.85	yes
isotropic nonlinear diffusion	8.03	9.59	yes
anisotropic nonlinear diffusion	7.25	9.19	yes
biharmonic smoothing	8.10	9.47	no
triharmonic smoothing	8.54	12.92	no

11

that the use of a novel interpolation technique based on anisotropic nonlinear diffusion with a diffusion tensor gives the most favourable results: It outperforms interpolation techniques based on radial basis functions, linear diffusion and isotropic nonlinear diffusion, Moreover, it allows discontinuity-preserving interpolation without visible oscillations. Provided that the tensor input data are positive semidefinite, this property is naturally inherited to its diffusion interpolant. This renders anisotropic nonlinear diffusion interpolation a highly interesting tool for applications such as diffusion tensor MRI.

In our future work, we head for a detailed theoretical analysis of these methods. We also plan to implement numerical methods with high efficiency, and study possible extensions. We will also investigate the usefulness of anisotropic nonlinear diffusion interpolation for lossy image compression. First results are reported in [8].

Acknowledgements

References

[1] A. Aldroubi and P. Basser. Reconstruction of vector and tensor fields from sampled discrete data. In D. Larson and L. Baggett, editors, *The Functional and Harmonic Analysis of Wavelets*, volume 247 of *Contemporary Mathematics*, pages 1–15. AMS, Providence, 1999.

[2] T. Brox, J. Weickert, B. Burgeth, and P. Mrázek. Nonlinear structure tensors. Technical Report 113, Dept. of Mathematics, Saarland University, Saarbrücken, Germany, October 2004.

[3] M. D. Buhmann. *Radial Basis Functions*. Cambridge University Press, Cambridge, UK, 2003.

[4] V. Caselles, J.-M. Morel, and C. Sbert. An axiomatic approach to image interpolation. *IEEE Transactions on Image Processing*, 7(3):376–386, March 1998.

[5] T. F. Chan and J. Shen. Non-texture inpainting by curvature-driven diffusions (CDD). *Journal of Visual Communication and Image Representation*, 12(4):436–449, 2001.

[6] P. Charbonnier, L. Blanc-Féraud, G. Aubert, and M. Barlaud. Two deterministic half-quadratic regularization algorithms for computed imaging. In *Proc. 1994 IEEE International Conference on Image Processing*, volume 2, pages 168–172, Austin, TX, November 1994. IEEE Computer Society Press.

[7] R. Franke. Scattered data interpolation: Tests of some methods. *Mathematics of Computation*, 38:181–200, 1982.

[8] I. Galić, J. Weickert, M. Welk, A. Bruhn, A. Belyaev, and H.-P. Seidel. Towards PDE-based image compression. Manuscript, June 2005. Submitted.

[9] H. Grossauer and O. Scherzer. Using the complex Ginzburg–Landau equation for digital impainting in 2D and 3D. In L. D. Griffin and M. Lillholm, editors, *Scale-Space Methods in Computer Vision*, volume 2695 of *Lecture Notes in Computer Science*, pages 225–236, Berlin, 2003. Springer.

[10] T. Lehmann, C. Gönner, and K. Spitzer. Survey: Interpolation methods in medical image processing. *IEEE Transactions on Medical Imaging*, 18(11):1049–1075, November 1999.

[11] F. Malgouyres and F. Guichard. Edge direction preserving image zooming: A mathematical and numerical analysis. *SIAM Journal on Numerical Analysis*, 39(1):1–37, 2001.

[12] S. Masnou and J.-M. Morel. Level lines based disocclusion. In *Proc. 1998 IEEE International Conference on Image Processing*, volume 3, pages 259–263, Chicago, IL, October 1998.

[13] E. Meijering. A chronology of interpolation: From ancient astronomy to modern signal and image processing. *Proceedings of the IEEE*, 90(3):319–342, March 2002.

[14] M. Moakher and P. G. Batchelor. Symmetric positive definite matrices: From geometry to applications and visualization. In J. Weickert and H. Hagen, editors, *Visualization and Processing of Tensor Fields*. Springer, Berlin, 2005.

[15] G. M. Nielson and J. Tvedt. Comparing methods of interpolation for scattered volumetric data. In D. F. Rogers and R. A. Earnshaw, editors, *State of the Art in Computer Graphics: Aspects of Visualization*, pages 67–86. Springer, New York, 1994.

[16] S. Pajevic, A. Aldroubi, and P. Basser. Continuous tensor field approximation of diffusion tensor MRI data. In J. Weickert and H. Hagen, editors, *Visualization and Processing of Tensor Fields*. Springer, Berlin, 2005.

[17] L. I. Rudin, S. Osher, and E. Fatemi. Nonlinear total variation based noise removal algorithms. *Physica D*, 60:259–268, 1992.

[18] E. Suarez-Santana, M. A. Rodriguez-Florido, C. Castaño-Moraga, C.-F. Westin, and J. Ruiz-Alzola. A generalized local structure measure to regularize tensor fields. In J. Weickert and H. Hagen, editors, *Visualization and Processing of Tensor Fields*. Springer, Berlin, 2005.

[19] D. Tschumperlé and R. Deriche. Orthonormal vector sets regularization with PDE's and applications. *International Journal of Computer Vision*, 50(3):237–252, December 2002.

[20] J. Weickert. *Anisotropic Diffusion in Image Processing*. Teubner, Stuttgart, 1998.

[21] J. Weickert and T. Brox. Diffusion and regularization of vector- and matrix-valued images. In M. Z. Nashed and O. Scherzer, editors, *Inverse Problems, Image Analysis, and Medical Imaging*, volume 313 of *Contemporary Mathematics*, pages 251–268. AMS, Providence, 2002.